AGU PUBLICATIONS

Geophysical Research Letters

RESEARCH LETTER
10.1002/2014GL061645

Key Points:
- Radar scattering shows upstream region with flow-aligned lineated bedforms
- Radar scattering shows downstream region with high bed roughness
- Morphologies are consistent with upstream sediments and downstream bedrock

Correspondence to:
D. M. Schroeder,
dustin.m.schroeder@utexas.edu

Citation:
Schroeder, D. M., D. D. Blankenship, D. A. Young, A. E. Witus, and J. B. Anderson (2014), Airborne radar sounding evidence for deformable sediments and outcropping bedrock beneath Thwaites Glacier, West Antarctica, *Geophys. Res. Lett.*, *41*, 7200–7208, doi:10.1002/2014GL061645.

Received 24 AUG 2014
Accepted 3 OCT 2014
Accepted article online 7 OCT 2014
Published online 24 OCT 2014

Airborne radar sounding evidence for deformable sediments and outcropping bedrock beneath Thwaites Glacier, West Antarctica

Dustin M. Schroeder[1], Donald D. Blankenship[1], Duncan A. Young[1], Alexandra E. Witus[2], and John B. Anderson[2]

[1]Institute for Geophysics, University of Texas, Austin, Texas, USA, [2]Department of Earth Sciences, Rice University, Houston, Texas, USA

Abstract The geologic and morphologic records of prior ice sheet configurations show evidence of rapid, back-stepping, meltwater intensive retreats. However, the potential for such a retreat in a contemporary glacier depends on the lithology of the current ice sheet bed, which lies beneath kilometers of ice, making its physical properties difficult to constrain. We use radar sounding and marine bathymetry data to compare the bed configuration of Thwaites Glacier to the bed of paleo-Pine Island Glacier. Using observed and modeled radar scattering, we show that the tributaries and upper trunk of Thwaites Glacier are underlain by ice flow-aligned bedforms consistent with deformable sediment and that the lower trunk is grounded on a region of high bed roughness consistent with outcropping bedrock. This is the same configuration as paleo-Pine Island Glacier during its retreat across the inner continental shelf.

1. Introduction

Thwaites Glacier lies in the Amundsen Sea Embayment (ASE) of the marine West Antarctic Ice Sheet (WAIS) and is one of the largest, most rapidly changing glaciers on Earth [*Chen et al*., 2009; *Lee et al*., 2012; *Rignot et al*., 2014]. Its landward sloping bed reaches into the deep interior of the ice sheet [*Holt et al*., 2006], making it a leading component in deglaciation scenarios [*Bamber et al*., 2009; *Joughin et al*., 2014]. Improved predictions of the contribution of the WAIS to future sea level require assessing the potential that Thwaites Glacier will experience an unstable retreat [*Solomon et al*., 2007]. The recent observed acceleration and mass loss in the ASE, in general, and the Thwaites Glacier catchment in particular are thought to be driven by the flux of warm ocean water reducing buttressing and melting ice near the grounding zone [*Pritchard et al*., 2012; *Rignot et al*., 2013]. The magnitude and sensitivity of the response to this forcing, however, will also depend on the geologic and geometric configurations of the contemporary ice sheet bed [*Alley*, 1989; *Blankenship et al*., 2001; *Jamieson et al*., 2012; *Parizek et al*., 2013].

Shipborne acoustic bathymetric mapping of paleoice streams on deglaciated continental shelves has been used to infer the configurations and processes associated with past ice sheet retreats [*O'Cofaigh and Pudsey*, 2002; *Lowe and Anderson*, 2002; *Wellner et al*., 2006; *Dowdeswell et al*., 2008; *Larter et al*., 2009; *Jakobsson et al*., 2012; *Nitsche et al*., 2013]. These observations show that Thwaites Glacier and Pine Island Glacier once converged on the outer continental shelf of the ASE, sharing a single grounding line as part of the paleo-Pine Island Glacier (Figure 1a). Morphologic and geologic records [*Lowe and Anderson*, 2003; *Graham et al*., 2010; *Kirshner et al*., 2012; *Jakobsson et al*., 2012; *Hillenbrand et al*., 2013; *Larter et al*., 2014; *Nitsche et al*., 2013; *Witus et al*., 2014] also show that paleo-Pine Island Glacier initially retreated across a region of deformable sediments, leaving ice-flow-aligned lineated bedforms (Figure 1c). After crossing a sedimentary to crystalline bed transition on the inner continental shelf (solid white line in Figure1a), the grounding line progressed in a rapid, back-stepping, meltwater intensive retreat across exposed bedrock (Figure 1b) with a network of interconnected channels [*Witus et al*., 2014; *Smith et al*., 2014]. Today, Pine Island Glacier is grounded inland of that bedrock region on a landward sloping bed [*Favier et al*., 2014] with actively eroding sediments [*Jenkins et al*., 2010; *Muto et al*., 2013; *Smith et al*., 2013].

Recent observations show that the grounding line of Thwaites Glacier has also been stepping back across a series of bedrock ridges and is currently grounded on one of them [*Tinto and Bell*, 2011]. The initiation and ultimate extent of a retreat from this position will be controlled by a combination of ocean forcing

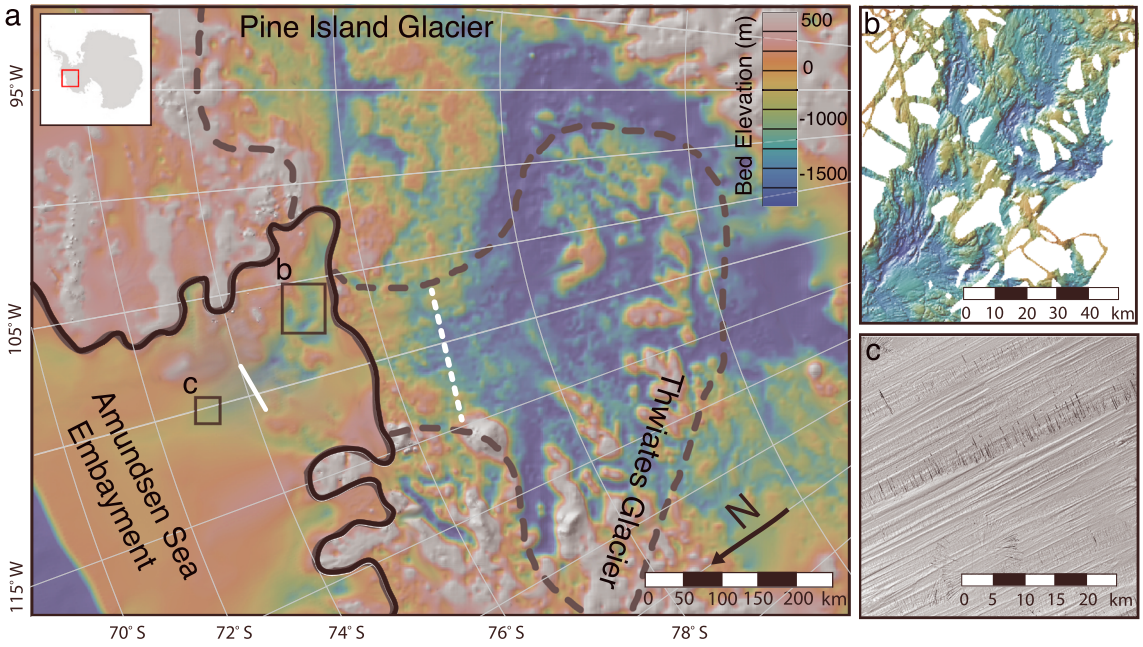

Figure 1. Bathymetry and bed topography [*Fretwell et al.*, 2013] of (a) the ASE, including the sediment to bedrock transition on the inner continental shelf (solid white line) [*Kirshner et al.*, 2012] and the distributed concentrated subglacial water system transition beneath Thwaites Glacier (dashed white line) [*Schroeder et al.*, 2013]. Bathymetry of (b) the exposed bedrock on the inner continental shelf *Nitsche et al.* [2013] and (c) the lineated sedimentary bedforms on the outer continental shelf [*Jakobsson et al.*, 2011; *Anderson and Jakobsson*, 2010]. The dashed black line shows the boundary of the Thwaites Glacier catchment.

[*Assmann et al.*, 2013; *Joughin et al.*, 2014], bed topography [*Holt et al.*, 2006; *Schoof*, 2007; *Jamieson et al.*, 2012], grounding zone hydrology [*Walker et al.*, 2013], geothermal flux [*Schroeder et al.*, 2014a, 2014b], and shear margin stability [*MacGregor et al.*, 2013] of Thwaites Glacier. However, the pacing and character of such a retreat will also depend on the geology of the bed upstream of the grounding line [*Blankenship et al.*, 2001; *Parizek et al.*, 2013; *Christianson et al.*, 2013; *Alley et al.*, 2007; *Anandakrishan et al.*, 2007].

2. Observing Subglacial Bedforms Using Airborne Radar Sounding

The marine bathymetry of the deglaciated bed of paleo-Pine Island Glacier (Figure 1a) provides two potential configurations for the contemporary bed of Thwaites Glacier. The first configuration includes a layer of deformable sediment that can form anisotropically rough ice-flow-aligned lineated bedforms [*Jakobsson et al.*, 2011]. This bed configuration is a characteristic of numerous paleoice streams [*Livingstone et al.*, 2012; *Spagnolo et al.*, 2014] including paleo-Pine Island Glacier from the Last Glacial Maximum to ~10.3 kya [*Kirshner et al.*, 2012] (seaward of the solid white line in Figure1a) as well as the contemptorary bed of the Rutford Ice Stream [*King et al.*, 2009]. The second configuration includes a bed of outcropping bedrock with a network of interconnected meltwater channels. This was the bed configuration for paleo-Pine Island Glacier ~7 kya [*Kirshner et al.*, 2012] (landward of the solid white line in Figure 1). Although, in some ways, these configurations represent end-members on the continuum of observed paleo-ice-sheet beds [e.g., *Wellner et al.*, 2006; *Bradwell et al.*, 2008; *Livingstone et al.*, 2012], their geographic proximity and geologic context make them plausible and informative hypotheses to test for the current bed of Thwaites Glacier.

Airborne [*Peters et al.*, 2005] and ground-based [*King et al.*, 2009] radar sounding systems have been used to directly image the topography and morphology of contemporary ice sheet beds. However, the physical scale of bedforms that can provide evidence of bed lithology (e.g., lineated deformable sediments) are often near or below the resolution of radar sounding systems. Further, the survey line spacing required to accurately track these bedforms between profiles is impractical for surveys that span the entire glacier catchments. Fortunately, the contrasting orientation-dependent roughness (at the radar scattering scale) of the two hypothesized bed configurations described above would be expressed in their orientation-dependent radar scattering signatures [*Peters et al.*, 2005]. Specifically, regions of the bed with lineated bedforms will be relatively smooth in the along-track direction when survey lines are aligned with bed form orientation

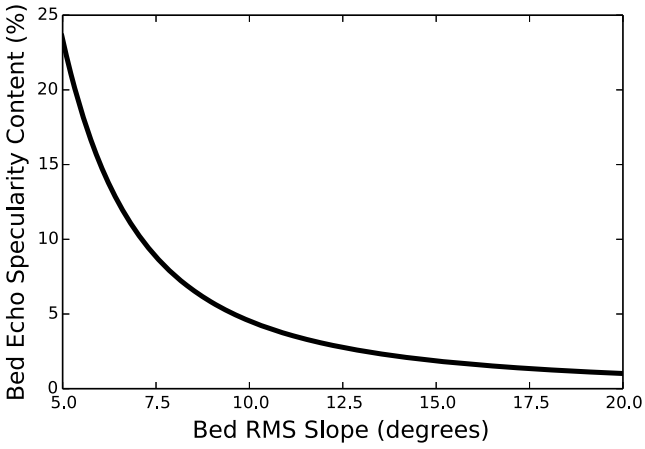

Figure 2. Bed echo specularity as a function of RMS slope of the bed for a survey height of 500 m, an ice thickness of 2 km, and focusing apertures of 700 m and 2000 m (typical values for data used in this study).

and relatively rough when they are perpendicular. By contrast, regions of the bed with high roughness (at the radar scattering scale) would appear rough in any survey orientation. This orientation-dependent (or independent) roughness would be expressed in the along-track scattering function and bed echo specularity [*Schroeder et al.*, 2014a, 2014b] with smoother bed regions producing more specular (or angularly narrow) bed echoes and rougher bed regions producing more diffuse (or angularly broad) bed echoes (Figure 2). Therefore, by focusing radar data collected with multiple apertures (after *Schroeder et al.* [2013]) and survey orientations, the orientation-dependent specularity of radar bed echoes can be measured and used to discriminate the radar scattering signatures of regions with ice flow-aligned lineated bedforms (relatively specular along flow and relatively diffuse across flow) from that of regions with high roughness (relatively diffuse in all orientations). Notably, this orientation-dependent specularity is sensitive to the meter-scale geometry of the bed [*Schroeder et al.*, 2014a, 2014b], which is below the imaging resolution of the radar [*Peters et al.*, 2007].

2.1. (An)Isotropy of Thwaites Glacier Bed Echo Specularity

Recent observations of subglacial water systems [*Schroeder et al.*, 2013] and modeling of basal shear stress [*Joughin et al.*, 2009] for Thwaites Glacier identify two distinct subglacial regions within its catchment. The first is the lower trunk region (downstream of the dashed white line in Figure 1a), which has relatively high basal shear stress [*Joughin et al.*, 2009] and channelized subglacial water [*Schroeder et al.*, 2013]. The second region includes the tributaries and upper trunk of Thwaites Glacier (upstream of the dashed white line in Figure 1a), which has relatively low basal shear stress [*Joughin et al.*, 2009] and distributed subglacial water [*Schroeder et al.*, 2013]. We first evaluate evidence for the lithology of these regions of the Thwaites Glacier bed by comparing their bed echo specularity in the two orthogonal survey directions (shown in Figure 3a).

The specularity content of radar bed echoes is a measure of the angular distribution of returned radar energy in the along-track direction and has been used to characterize subglacial water systems [*Schroeder et al.*, 2013]. By computing focused bed echo energies (E_1 and E_2) using two different aperture lengths (L_1 and L_2)

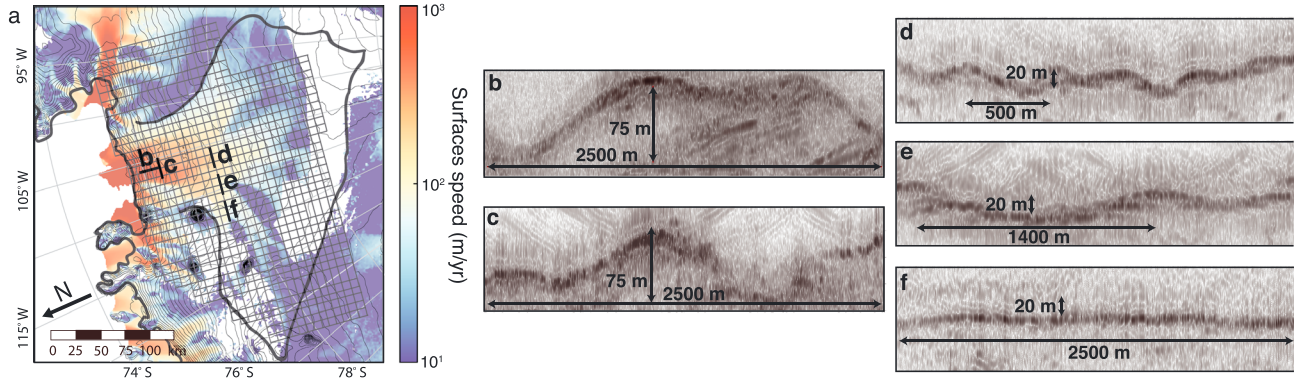

Figure 3. Radar profiles from an airborne survey of (a) the Thwaites Glacier catchment showing (b) the along-flow and (c) across-flow bedforms of the downstream region as well as (d) the across-flow, (e) oblique-to-flow, and (f) along-flow bedforms of the upstream region.

Table 1. Orientation-Dependent Specularity (%)

	Mean	Standard Deviation	Number of Observations	Anisotropy
Upstream Thwaites bed				
Parallel to ice flow	12.1	8.2	10,854	0.41
Perpendicular to ice flow	8.0	6.7	5,930	
Downstream Thwaites bed				
Parallel to ice flow	9.4	6.0	6,051	0.09
Perpendicular to ice flow	8.0	6.5	5,262	

[*Peters et al.*, 2007], which span two different ranges of scattering angles (φ_1 and φ_2), we compute the distributed energy (D) in the bed echo as

$$D = \frac{180^\circ}{\varphi_2 - \varphi_1}(E_2 - E_1), \tag{1}$$

the specular component of the bed echo as

$$S = E_2 - D\frac{\varphi_2}{180^\circ} = E_2 - D\frac{\varphi_1}{180^\circ}, \tag{2}$$

and the specularity content S_c as

$$S_c = \frac{S}{S + D}. \tag{3}$$

The orthogonal configuration of the radar sounding survey used in this work [*Holt et al.*, 2006] makes it possible to compare the bed echo specularity content in perpendicular directions. We determine the specularity content for north-south (S_{NS}) and east-west (S_{EW}) survey directions and produce gridded specularity maps (with 5×5 km grid cells) for each survey direction. Using these two gridded data sets, we calculate the anisotropy (A) and average specularity (S_{ave}) for each cell as

$$A = \frac{|S_{NS} - S_{EW}|}{(S_{NS} + S_{EW})/2} \tag{4}$$

and

$$S_{ave} = (S_{NS} + S_{EW})/2. \tag{5}$$

We compare the specularity values for grid cells where the survey orientations are parallel and perpendicular to ice flow. To select the cells where the observed specularity values are parallel and perpendicular to ice flow, we calculated the observation angle (Θ_{obs}) for each survey line as

$$\Theta_{obs} = \Theta_{line} - \Theta_{ice}, \tag{6}$$

where Θ_{line} is the direction of the airborne survey line and Θ_{ice} is the direction of ice flow from interferometric synthetic aperture radar-derived surface velocities [*Rignot et al.*, 2011]. We then selected the cells where one survey direction had an observation angle of $0^\circ \pm 5^\circ$ (and the other had an observation angle of $\pm 90^\circ \pm 5^\circ$) and the average specularity was less than 17.5% (expressing the geometry of bedforms rather than subglacial water networks [*Schroeder et al.*, 2014a, 2014b]). Table 1 also shows the values of the anisotropy of the specularity (A) for the upstream and downstream regions. These values show that the bed echo specularity of the upstream region is relatively anisotropic ($A = 0.41$) and is higher when the observation is aligned with ice flow ($\Theta_{obs} = 0^\circ$) and that the bed echo specularity of the downstream region is relatively isotropic ($A = 0.09$). This is consistent with the presence of flow-aligned lineated bedforms upstream and a region of high bed roughness downstream.

3. Radar Imagery of Bedforms

We present focused radar profiles (Figures 3b–3f) from the airborne radar sounding survey of the catchment (Figure 3a) [*Holt et al.*, 2006] and compare these profiles of subglacial bedforms to the rough outcropping bedrock (Figure 1b) and lineated sediments (Figure 1c) observed by shipborne acoustic bathymetry of the ASE continental shelf [*Anderson and Jakobsson*, 2010; *Jakobsson et al.*, 2011; *Nitsche et al.*, 2013]. In the upstream region of the Thwaites Glacier bed, radar profiles collected perpendicular (Figure 3d), oblique

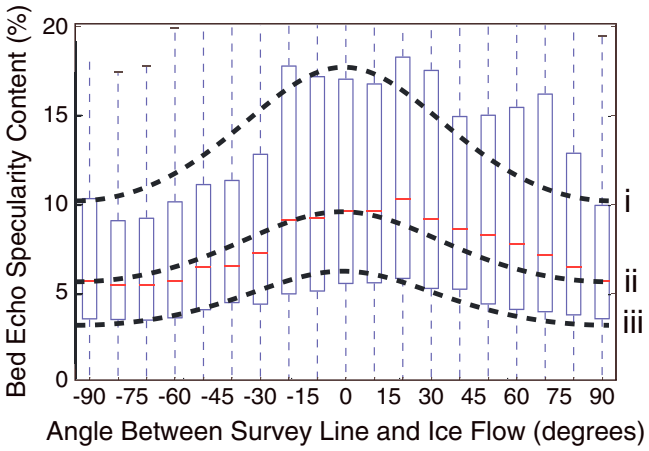

Figure 4. Box plots of angularly dependent specularity for the upstream regions of the Thwaites Glacier bed. The red lines show the medians, the blue boxes span the interquartile ranges, and the blue dashed lines extend to the full ranges of values. The black dashed lines show the analytic specularity response for a sinusoidally corrugated sedimentary bed with height to width ratios and surface texture RMS slopes of (a) 0.3 and 6°, (b) 0.4 and 7°, and (c) 0.7 and 8°.

(Figure 3e), and parallel (Figure 3f) to ice flow show a corrugated bed with crest-to-trough heights (H) of ~20 m and crest-to-crest widths (w) of ~500 m. These corrugations are similar in scale to lineated sedimentary bedforms (i.e., mega-scale glacial lineations) observed elsewhere beneath contemporary and paleoice sheets [*King et al.*, 2009; *Jakobsson et al.*, 2011; *Livingstone et al.*, 2012; *Spagnolo et al.*, 2014]. In the downstream region, the along-flow (Figure 3b) and across-flow (Figure 3c) radar profiles show bedforms that are rough in both survey directions and have physical scales and morphologies consistent with the deglaciated outcropping bedrock on the inner continental shelf of the ASE (Figure 1b). Collectively, these radar profiles support the interpretation that the observed variation in specularity is the result of lineated bed form upstream and a region of high bed roughness downstream.

4. Constraining Bed Form Geometry With Orientation-Dependent Specularity

For the ice flow-aligned lineated bedforms in the upstream region of the Thwaites Glacier bed, the angularly dependent specularity is an expression of meter-scale bed form geometry [*Schroeder et al.*, 2014a, 2014b; *Peters et al.*, 2005]. Plotting the specularity of bed echoes for the upstream region as a function of observation angle (Θ_{obs}) (Figure 4) shows that the specularity varies smoothly with angle and has the highest values parallel to ice flow ($\Theta_{obs} = 0°$) and the lowest values perpendicular to ice flow ($\Theta_{obs} = \pm 90°$) (these correspond to the parallel and perpendicular specularity values in Table 1). To constrain the physical scale of the bed forms producing the pattern of orientation-dependent specularity in the upstream region of the bed, we compare those values to a set (Figures 4a–4c) of simple two-scale radar scattering models [*Ogilvy*, 1991] for a bed that is sinusoidally corrugated at large (greater than tens of meters) scales and has a rough surface texture at small (less than a meter) scales.

In these models, the bed is defined by the ratio of the crest-to-trough height (H) to the crest-to-crest width (w) and the surface texture root-mean-square (RMS) slope ($\sigma_{texture}$). As the observation angle (Θ_{obs}) changes, the along-track profiles of the bed can be modeled as sine waves with an orientation-dependent height-to-width ratio (H/w_Θ) of

$$\frac{H}{w_\Theta} = \frac{H}{w}\left(\frac{1}{\sin\Theta_{obs}}\right), \tag{7}$$

which corresponds to a bed form-scale RMS slope (σ_{bed}) of

$$\sigma_{bed} = \tan^{-1}\left(\frac{\pi}{\sqrt{2}}\,\frac{H}{w}\sin\Theta_{obs}\right) \tag{8}$$

and a total combined (both bed form and surface texture) RMS slope σ_{total} [*Ogilvy*, 1991] of

$$\sigma_{total} = \sqrt{{\sigma_{bed}}^2 + {\sigma_{texture}}^2}. \tag{9}$$

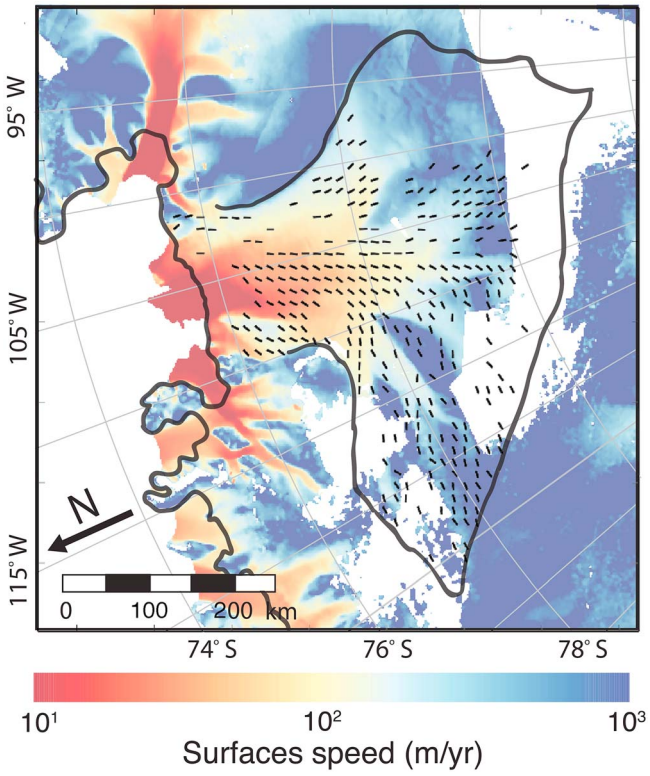

Figure 5. Axis of symmetry for anisotropic specularity (aligned with black dashes) in areas with low-average specularity in the context of ice flow [*Rignot et al.*, 2011].

We model the return from this surface as a Gaussian scattering function [*Nayar et al.*, 1991; *MacGregor et al.*, 2013] so that the echo energy E_i focused with an aperture that spans a range of scattering angles (φ_i) is proportional to

$$E_i \propto \mathrm{erf}\left(\frac{\varphi_i}{\sigma_{\mathrm{total}}}\right), \tag{10}$$

where erf is the error function. Then, the specularity content (S_c) of radar echoes from 203, the modeled sinusoidally corrugated bed is given by equations (1–3).

Comparing the observed orientation-dependent specularity of the upstream region of the Thwaites Glacier bed (Figure 4) to these models (Figures 4a–4c) puts constraints on the geometry lineated bed forms of height-to-width ratios between 0.3 and 0.7 and surface texture RMS slopes between 6° and 8°. These values are consistent with the geometry of mega-scale glacial lineations observed offshore [*Jakobsson et al.*, 2011; *Spagnolo et al.*, 2014] and beneath contemporary ice sheets [*King et al.*, 2009] (Figures 3d–3f) as well as the roughness of sedimentary surfaces [*Shepard et al.*, 2001].

5. Bed Form Orientation From Anisotropic Specularity

Since the radar only profiles along flight lines, which are separated by 15 km, we use the anisotropy of radar scattering to determine the distribution and orientation of flow-aligned bed forms across the catchment. By calculating the specularity content for both survey directions (S_{NS} and S_{EW}) and producing two orthogonal gridded specularity maps, we calculated the axis of symmetry of the specularity (Θ_{spec}) (which corresponds to bed form orientation) for each cell as

$$\Theta_{\mathrm{spec}} = \tan^{-1}(S_{\mathrm{EW}}/S_{\mathrm{NS}}). \tag{11}$$

We resolve the ambiguity in the direction of Θ_{spec} (resulting from the $\tan^{-1}$) by mirroring the direction across the center line of the glacier, which produces values that vary smoothly across the catchment and prevents physically unrealistic discontinuities and divergence. For grid cells that have both anisotropic specularity ($A > 0.4$) and lower average specularity (S_{ave}), we plot the radar-derived bed form orientation (Θ_{spec}) in the context of the ice surface speed [*Rignot et al.*, 2011] (Figure 5). This shows that bed form orientations generally align with ice flow in the upper trunk and tributaries of the Thwaites Glacier catchment.

6. Discussion

The morphology of the upstream region of the contemporary Thwaites Glacier bed produces anisotropic radar scattering (Table 1) with orientation-dependent specularity (Figure 4) consistent with flow-aligned (Figure 5) sinusoidally corrugated bed forms on the scale of those visible in radar profiles (Figure 3). The radar scattering signature of the upstream region is also consistent with the physical scale and morphology of

lineated bed forms of deformable sediment observed on the outer continental shelf of the ASE (Figure 1c). Although there are examples of anisotropically rough lineated bedrock in paleo-ice-stream regions [*Bradwell et al*., 2008; *Rippin et al*., 2014], the height-to-width ratios of these features are too high to produce orientation-dependent specularity values observed for the upstream region (Figure 4) and would instead produce isotropically rough scattering values (Figure 2) like those observed for the downstream region (Table 1). Therefore, we interpret these radar scattering signatures as evidence that the upstream region of the Thwaites Glacier bed is underlain by lineated bed forms, mega-scale glacial lineations overprinting deformable sediments, like those observed on the outer continental shelf of the ASE (Figure 1c) and that the in downstream region is underlain by outcropping bedrock like that observed on the inner continental shelf of the ASE (Figure 1b). This hypothesis is consistent with the local geology (outcropping bedrock of the ASE adjacent to the downstream region [*Lowe and Anderson*, 2002] and deformable sediments of the Siple Coast adjacent to upstream region [*Blankenship et al*., 2001]) and glaciology (concentrated water with high basal shear downstream and distributed water with low basal upstream [*Joughin et al*., 2009; *Schroeder et al*., 2013]) and could be tested using drilling or seismic data.

7. Conclusions

We conclude that the tributaries and upper trunk of Thwaites Glacier are underlain by ice flow-aligned lineated bed forms with height-to-width ratios between 0.3 and 0.7 and surface texture RMS slopes between 6° and 8°. We also conclude that the lower trunk is grounded on a region of high bed roughness. This is consistent with a bed configuration of deformable sediments (like those observed on the outer continental shelf of the ASE) in the upstream region and outcropping bedrock lacking any significant sediment cover (like that observed on the inner shelf of the ASE) in the downstream region. This is the same bed configuration as paleo-Pine Island Glacier during its meltwater intensive retreat across the exposed bedrock on the inner continental shelf.

Acknowledgments

Radar processing assistance was provided by S. Kempf and radar interpretation was performed by J. DeSanto, A. Jones, E. Powell, and M. Williams. We thank N. Ross and several anonymous reviewers for their constructive feedback. We thank the National Science Foundation (grant numbers PLR-0636724 and CDI-0941678 to D.D.B. and ANT-0837925 to J.B.A.), the National Aeronautics and Space Administration (grant number NNX08AN68G to D.D.B.), and the G. Unger Vetlesen Foundation for supporting this work. D.M.S. received support from a NSF GRFP Fellowship, a University of Texas Recruiting Fellowship, and the UTIG Gale White Fellowship. Data will been made available through the National Snow and Ice Data Center. This is UTIG contribution 2734.

The Editor thanks two anonymous reviewers for their assistance in evaluating this paper.

References

Alley, R. B. (1989), Water-pressure coupling of sliding and bed deformation: I. Water system, *J. Glaciol.*, *35*(119), 108–118, doi:10.3189/002214389793701527.

Alley, R. B., S. Anandakrishnan, T. K. Dupont, B. R. Parizek, and D. Pollard (2007), Effect of sedimentation on ice-sheet grounding-line stability, *Science*, *315*(5820), 1838–41, doi:10.1126/science.1138396.

Anandakrishnan, S., G. A. Catania, R. B. Alley, and H. J. Horgan (2007), Discovery of till deposition at the grounding line of Whillans Ice Stream, *Science*, *315*(5820), 1835–1838.

Anderson, J. B., and M. Jakobsson (2010), Oden Southern Ocean 0910, OSO 0910: Cruise report, *Meddelanden fran Stockholms Universitets Institution för Gelogiska Vetenskaper 341*. [Available at http://su.diva-portal.org/smash/get/diva2:383008/FULLTEXT01.pdf.]

Assmann, K. M., A. Jenkins, D. R. Shoosmith, D. P. Walker, S. S. Jacobs, and K. W. Nicholls (2013), Variability of Circumpolar Deep Water transport onto the Amundsen Sea Continental shelf through a shelf break trough, *J. Geophys. Res. Oceans*, *118*, 6603–6620, doi:10.1002/2013JC008871.

Bamber, J. L., R. E. M. Riva, B. L. A. Vermeersen, and A. M. Le Brocq (2009), Reassessment of the potential sea-level rise from a collapse of the West Antarctic ice sheet, *Science*, *324*(5929), 901–903, doi:10.1126/science.1169335.

Blankenship, D. D., D. L. Morse, C. A. Finn, R. E. Bell, M. E. Peters, S. D. Kempf, S. M. Hodge, M. Studinger, J. C. Behrendt, and J. M. Brozena (2001), Geologic controls on the initiation of rapid basal motion for West Antarctic ice streams: A geophysical perspective including new airborne radar sounding and laser altimetry results, in *The West Antarctic Ice Sheet: Behavior and Environment*, *Antarct. Res. Ser*., vol. 77, edited by R. B. Alley and R. A. Bindschadler, pp. 105–121, AGU, Washington, D. C.

Bradwell, T., M. Stoker, and M. Krabbendam (2008), Megagrooves and streamlined bedrock in NW Scotland: The role of ice streams in landscape evolution, *Geomorphology*, *97*, 135–156, doi:10.1016/j.geomorph.2007.02.040.

Chen, J. L., C. R. Wilson, D. D. Blankenship, and B. D. Tapley (2009), Accelerated Antarctic ice loss from satellite gravity measurements, *Nat. Geosci.*, *2*(12), 859–862.

Christianson, K., B. R. Parizek, R. B. Alley, H. J. Horgan, R. W. Jacobel, S. Anandakrishnan, B. A. Keisling, B. D. Craig, and A. Muto (2013), Ice sheet grounding zone stabilization due to till compaction, *Geophys. Res. Lett.*, *40*, 5406–5411, doi:10.1002/2013GL057447.

Dowdeswell, J. A., D. Ottesen, J. Evans, C. O'Cofaigh, and J. B. Anderson (2008), Submarine glacial landforms and rates of ice-stream collapse, *Geology*, *36*(10), 819, doi:10.1130/G24808A.1.

Favier, L., G. Durand, S. Cornford, G. Gudmundsson, O. Gagliardini, F. Gillet-Chaulet, T. Zwinger, A. Payne, and A. Le Brocq (2014), Retreat of Pine Island Glacier controlled by marine ice-sheet instability, *Nat. Clim. Change*, *4*, 117–121, doi:10.1038/nclimate2094.

Fretwell, P., et al. (2013), Bedmap2: Improved ice bed, surface and thickness datasets for Antarctica, *The Cryosphere*, *7*(1), 375–393.

Graham, A. G., R. D. Larter, K. Gohl, J. A. Dowdeswell, C.-D. Hillenbrand, J. A. Smith, J. Evans, G. Kuhn, and T. J. Deen (2010), Flow and retreat of the late quaternary Pine Island-Thwaites palaeo-ice stream, West Antarctica, *J. Geophys. Res.*, *115*, F03025, doi:10.1029/2009JF001482.

Hillenbrand, C.-D., et al. (2013), Grounding-line retreat of the West Antarctic Ice Sheet from inner Pine Island Bay, *Geology*, *41*(1), 35–38.

Holt, J. W., D. D. Blankenship, D. L. Morse, D. A. Young, M. E. Peters, S. D. Kempf, T. G. Richter, D. G. Vaughan, and H. F. J. Corr (2006), New boundary conditions for the West Antarctic Ice Sheet: Subglacial topography of the Thwaites and Smith glacier catchments, *Geophys. Res. Lett.*, *33*, L09502, doi:10.1029/2005GL025561.

Jakobsson, M., et al. (2011), Geological record of ice shelf break-up and grounding line retreat, Pine Island Bay, West Antarctica, *Geology*, *39*(7), 691–694, doi:10.1130/G32153.1.

Jakobsson, M., J. B. Anderson, F. O. Nitsche, R. Gyllencreutz, A. E. Kirshner, N. Kirchner, M. O'Regan, R. Mohammad, and B. Eriksson (2012), Ice sheet retreat dynamics inferred from glacial morphology of the central Pine Island Bay Trough, West Antarctica, *Quat. Sci. Rev.*, *38*, 1–10, doi:10.1016/j.quascirev.2011.12.017.

Jamieson, S. S. R., A. Vieli, S. J. Livingstone, C. O'Cofaigh, C. Stokes, C. D. Hillenbrand, and J. A. Dowdeswell (2012), Ice-stream stability on a reverse bed slope, *Nat. Geosci.*, *5*, 799–802, doi:10.1038/NGEO1600.

Jenkins, A., P. Dutrieux, S. S. Jacobs, S. D. McPhail, J. R. Perrett, A. T. Webb, and D. White (2010), Observations beneath Pine Island glacier in West Antarctica and implications for its retreat, *Nature*, *3*(7), 468–472, doi:10.1038/ngeo890.

Joughin, I. R., S. Tulaczyk, J. L. Bamber, D. D. Blankenship, J. W. Holt, T. Scambos, and D. G. Vaughan (2009), Basal conditions for Pine Island and Thwaites Glaciers, West Antarctica, determined using satellite and airborne data, *J. Glaciol.*, *55*(190), 245–257, doi:10.3189/002214309788608705.

Joughin, I., B. E. Smith, and B. Medley (2014), Marine ice sheet collapse potentially under way for the Thwaites glacier basin, West Antarctica, *Science*, *344*(6185), 735–738.

King, E. C., R. C. A. Hindmarsh, and C. C. R. Stokes (2009), Formation of mega-scale glacial lineations observed beneath a West Antarctic ice stream, *Nat. Geosci.*, *2*(8), 585–588, doi:10.1038/ngeo581.

Kirshner, A., J. Anderson, M. Jakobsson, M. O'Regan, W. Majewski, and F. Nitsche (2012), Post-LGM deglaciation in Pine Island Bay, West Antarctica, *Quat. Sci. Rev.*, *38*, 11–26, doi:10.1016/j.quascirev.2012.01.017.

Larter, R. D., A. G. Graham, and K. Gohl (2009), Subglacial bedforms reveal complex basal regime in a zone of paleo–ice stream convergence, Amundsen sea embayment, West Antarctica, *Geology*, *37*(5), 411–414, doi:10.1130/G25505A.1.

Larter, R. D., et al. (2014), Reconstruction of changes in the Amundsen Sea and Bellingshausen sea sector of the West Antarctic ice sheet since the last glacial maximum, *Quat. Sci. Rev.*, *100*, 55–86, doi:10.1016/j.quascirev.2013.10.016.

Lee, H., C. Shum, I. M. Howat, A. Monaghan, Y. Ahn, J. Duan, J.-Y. Guo, C.-Y. Kuo, and L. Wang (2012), Continuously accelerating ice loss over Amundsen sea catchment, West Antarctica, revealed by integrating altimetry and GRACE data, *Earth Planet. Sci. Lett.*, *321–322*, 74–80, doi:10.1016/j.epsl.2011.12.040.

Livingstone, S. J., C. O. Cofaigh, C. R. Stokes, C.-D. Hillenbrand, A. Vieli, and S. S. R. Jamieson (2012), Antarctic paleo-ice streams, *Earth Sci. Rev.*, *111*, 90–128, doi:10.1016/j.earscirev.2011.10.003.

Lowe, A. L., and J. B. Anderson (2002), Reconstruction of the West Antarctic ice sheet in Pine Island Bay during the last glacial maximum and its subsequent retreat history, *J. Glaciol.*, *49*(164), 1879–1897, doi:10.1016/S0277-3791(02)00006-9.

Lowe, A. L., and J. B. Anderson (2003), Evidence for abundant subglacial meltwater beneath the paleo-ice sheet in Pine Island Bay, Antarctica, *J. Glaciol.*, *49*(164), 125–138, doi:10.3189/172756503781830971.

MacGregor, J. A., G. A. Catania, H. Conway, D. M. Schroeder, I. Joughin, D. A. Young, S. D. Kempf, and D. D. Blankenship (2013), Weak bed control of the eastern shear margin of Thwaites Glacier, West Antarctica, *J. Glaciol.*, *59*(217), 900–912, doi:10.3189/2013JoG13J050.

Muto, A., S. Anandakrishnan, and R. B. Alley (2013), Subglacial bathymetry and sediment layer distribution beneath the Pine Island Glacier ice shelf, West Antarctica, modeled using aerogravity and autonomous underwater vehicle data, *Ann. Glaciol.*, *54*(64), 27–32, doi:10.3189/2013AoG64A110.

Nayar, S., K. Ikeuchi, and T. Kanade (1991), Surface reflection: Physical and geometrical perspectives, *IEEE Trans. Pattern Anal.*, *13*(7), 611–634.

Nitsche, F. O., K. Gohl, R. D. Larter, C.-D. Hillenbrand, G. Kuhn, J. A. Smith, S. Jacobs, J. B. Anderson, and M. Jakobsson (2013), Paleo ice flow and subglacial meltwater dynamics in Pine Island Bay, West Antarctica, *The Cryosphere*, *7*(1), 249–262, doi:10.5194/tc-7-249-2013.

O'Cofaigh, C., and C. Pudsey (2002), Evolution of subglacial bedforms along a paleo-ice stream, Antarctic Peninsula continental shelf, *Geophys. Res. Lett.*, *29*(8), 1–4, doi:10.1029/2001GL014488.

Ogilvy, J. A. (1991), *Theory of Wave Scattering From Random Rough Surfaces*, A. Hilger, Bristol, U. K.

Parizek, B. R., et al. (2013), Dynamic instability of Thwaites glacier, West Antarctica, *J. Geophys. Res. Earth Surface*, *118*, 638–655, doi:10.1002/jgrf.20044.

Peters, M. E., D. D. Blankenship, and D. L. Morse (2005), Analysis techniques for co- herent airborne radar sounding: Application to West Antarctic ice streams, *J. Geophys. Res.*, *110*, B06303, doi:10.1029/2004JB003222.

Peters, M. E., D. D. Blankenship, S. P. Carter, S. D. Kempf, D. A. Young, and J. W. Holt (2007), Along-track focusing of airborne radar sounding data from West Antarctica for improving basal reflection analysis and layer detection, *IEEE Trans. Geosci. Remote Sens.*, *45*(9), 2725–2736, doi:10.1109/TGRS.2007.897416.

Pritchard, H. D., S. R. M. Ligtenberg, H. A. Fricker, D. G. Vaughan, M. R. van den Broeke, and L. Padman (2012), Antarctic ice-sheet loss driven by basal melting of ice shelves, *Nature*, *484*(7395), 502–5, doi:10.1038/nature10968.

Rignot, E., J. Mouginot, and B. Scheuchl (2011), Ice flow of the Antarctic ice sheet, *Science*, *333*(6048), 1427–1430, doi:10.1126/science.1208336.

Rignot, E., S. Jacobs, J. Mouginot, and B. Scheuchl (2013), Ice-shelf melting around Antarctica, *Science*, *341*(6143), 266–270, doi:10.1126/science.1235798.

Rignot, E., J. Mouginot, M. Morlighem, H. Seroussi, and B. Scheuchl (2014), Widespread, rapid grounding line retreat of Pine Island, Thwaites, Smith, and Kohler glaciers, West Antarctica, from 1992 to 2011, *Geophys. Res. Lett.*, *41*, 3502–3509, doi:10.1002/2014GL060140.

Rippin, D. M., R. G. Bingham, T. A. Jordan, A. P. Wright, N. Ross, H. F. J. Corr, F. Ferraccili, A. M. Le Brocq, K. C. Rose, and M. J. Siegert (2014), Basal roughness of the Institute and Moeller Ice Streams, West Antarctica: Process determination and landscape interpretation, *Geomorphology*, *214*, 139–147, doi:10.1016/j.geomorph.2014.01.021.

Schoof, C. G. (2007), Ice sheet grounding line dynamics: Steady states, stability, and hysteresis, *J. Geophys. Res.*, *112*, F03S28, doi:10.1029/2006JF000664.

Schroeder, D. M., D. D. Blankenship, and D. A. Young (2013), Evidence for a water system transition beneath Thwaites Glacier, West Antarctica, *Proc. Natl. Acad. Sci. U.S.A.*, *110*(30), 12,225–12,228, doi:10.1073/pnas.1302828110.

Schroeder, D. M., D. D. Blankenship, D. A. Young, and E. Quartini (2014a), Evidence for elevated and spatially variable geothermal flux beneath the West Antarctic Ice Sheet, *Proc. Natl. Acad. Sci. U.S.A.*, doi:10.1073/pnas.1405184111.

Schroeder, D. M., D. D. Blankenship, R. K. Raney, and C. Grima (2014b), Estimating subglacial water geometry using radar bed echo specularity: Application to Thwaites Glacier, West Antarctica, *IEEE Geosci. Remote Sens. Lett.*, *12*(3), 443–447, doi:10.1109/LGRS.2014.2337878.

Shepard, M. K., B. A. Campbell, M. H. Bulmer, T. G. Farr, L. R. Gaddis, and J. J. Plaut (2001), The roughness of natural terrain: A planetary and remote sensing perspective, *J. Geophys. Res.*, *106*, 777–795, doi:10.1029/2000JE001429.

Smith, A. J., C. D. Hillenbrand, G. Kuhn, J. P. Klages, A. G. C. Graham, R. D. Larter, W. Ehrmann, S. G. Moreton, S. Wiers, and T. Frederichs (2014), New constraints on the timing of West Antarctic Ice Sheet retreat in the eastern Amundsen sea since the last glacial maximum, *Global Planet. Change*, doi:10.1016/j.gloplacha.2014.07.015.

Smith, A. M., T. A. Jordan, F. Ferraccioli, and R. G. Bingham (2013), Influence of subglacial conditions on ice stream dynamics: Seismic and potential field data from Pine Island Glacier, West Antarctica, *J. Geophys. Res. Solid Earth*, *118*, 1471–1482, doi:10.1029/2012JB009582.

Solomon, S., D. Qin, M. Manning, Z. Chen, M. Marquis, K. B. Averyt, M. Tignor, and H. L. Miller (2007), The physical science basis, contribution of working group I to the fourth assessment report of the intergovernmental panel on climate change, pp. 235–337.

Spagnolo, M., C. D. Clark, J. C. Ely, C. R. Stokes, J. B. Anderson, K. Andreassen, A. G. Graham, and E. C. King (2014), Size, shape and spatial arrangement of mega-scale glacial lineations from a large and diverse dataset, *Earth Surf. Processes Landforms*, *39*(11), 1432–1448, doi:10.1002/esp.3532.

Tinto, K. J., and R. E. Bell (2011), Progressive unpinning of Thwaites Glacier from newly identified offshore ridge: Constraints from aerogravity, *Geophys. Res. Lett.*, *38*, L20503, doi:10.1029/2011GL049026.

Walker, R. T., B. R. Parizek, R. B. Alley, S. Anandakrishnan, K. L. Riverman, and K. Christianson (2013), Ice-shelf tidal flexure and subglacial pressure variations, *Earth Planet. Sci. Lett.*, *361*, 422–428, doi:10.1016/j.epsl.2012.11.008.

Wellner, J., D. Heroy, and J. B. Anderson (2006), The death mask of the Antarctic ice sheet: Comparison of glacial geomorphic features across the continental shelf, *Geomorphology*, *75*(1–2), 157–171, doi:10.1016/j.geomorph.2005.05.015.

Witus, A. E., C. M. Branecky, J. B. Anderson, W. Szczuciniski, D. M. Schroeder, D. D. Blankenship, and M. Jakobsson (2014), Meltwater intensive glacial retreat in polar environments and investigation of associated sediments: Example from Pine Island Bay, West Antarctica, *Quat. Sci. Rev.*, *85*, 99–118.